PAPER

Low-Cost Perturbation-Based ICI Equalizers for OFDMA Mobile Systems

Hsin-De LIN[†a)], ***Student Member***, **Tzu-Hsien SANG**[†], ***and*** **Jiunn-Tsair CHEN**[††], ***Nonmembers***

SUMMARY For advanced mobile communication systems that adopt orthogonal frequency-division multiple access (OFDMA) technologies, intercarrier interference (ICI) significantly degrades performance when mobility is high. Standard specifications and concerns about complexity demand low-cost methods with deployment readiness and decent performance. In this paper, novel zero forcing (ZF) and minimum mean-square error (MMSE) equalizers based on per-subcarrier adaptive (PSA) processing and perturbation-based (PB) approximation are introduced. The proposed equalizers strike a good balance between implementation cost and performance; therefore they are especially suitable for OFDMA downlink receivers. Theoretical analysis and simulations are provided to verify our claims.

key words: *orthogonal frequency-division multiple access (OFDMA), doubly-selective fading channel, intercarrier interference (ICI), ICI cancellation*

1. Introduction

Advanced OFDMA mobile systems, such as LTE and WiMAX, have to meet the challenges of achieving higher spectral efficiency and ability to operate in harsh environments. Usually high spectral efficiency in such systems is achieved by tightly squeezing subcarriers into a limited bandwidth [1]. This in turn implies that, when operating in a high-mobility scenario, for example on a high-speed vehicle, the channel exhibits fast fading and the signal experiences channel variation within one OFDMA symbol. Consequently, the channel frequency response (CFR) matrix in the transmission model is no longer diagonal, and off-diagonal terms contribute to severe intercarrier interference (ICI). As a result, a serious performance degradation may ensue if ICI is left untreated.

ICI cancellation for OFDM/OFDMA systems has been an active research topic for many years. Well-known methods abound (please see [2]–[15] and references therein). In [2], [4], [5], [9], frequency-domain zero forcing (ZF) or minimum mean-square error (MMSE) ICI equalizers are proposed, while time-domain equalizers are investigated in [3], [16]. For these methods, the major computational cost comes from matrix inversion. A common means to reduce the cost is to approximate the non-diagonal CFR matrix with a banded matrix in which all but few elements on selected $2Q + 1$ diagonals are set to zero [2], [4], [6], [9], [15]. With the banded structure, simpler matrix inversions are used to calculate MMSE or ZF ICI equalizer coefficients. A rule of thumb in choosing the bandwidth parameter Q is $Q \geq \lceil f_D/\Delta f \rceil + 1$, where f_D is the maximum Doppler frequency and Δf denotes the subcarrier spacing [6], [9]. However, the BER performance can degrade severely when Q is not large enough.

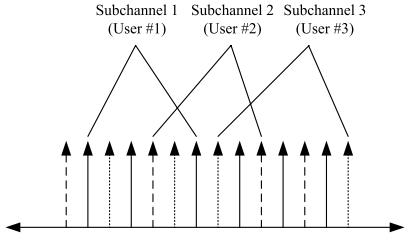

Fig. 1 OFDMA frequency description of PUSC mode.

Other than computational cost, features specified in advanced systems that were derived from WiMAX (IEEE 802.16e) [1] and LTE can also impose serious difficulties on engineering development. For instance, in Fig. 1 an example of subcarrier assignment under the mandatory mode of partial usage of subchannels (PUSC) in 802.16e is shown [1]. The usable subcarriers are divided into subsets denoted as subchannels. In the downlink, different users or groups of users may share the same subchannels. A user can end up using subcarriers interlaced with the subcarriers of other users. As a result, decision feedback equalizers (DFEs) [4], [6], [16] may not be appropriate for this situation, since its good performance relies on removing ICI induced by the user itself as well as by other users, which in turns requires the knowledge of CFR and data on un-occupied or other users' subcarriers. Under this circumstance, however, conventional linear equalizers can still be effective in mitigating ICI by inverting estimated CFR matrices with the help of pilots. Other sophisticated ICI cancellation techniques also face a variety of challenges restricting their deployment. The turbo ICI equalizer [10]–[12] requires CFR information and feedback from the channel decoder, and it has longer processing latency. Techniques that utilize time-domain windowing [6], [7] are effective for a large Doppler spread range but the receiver has to deal with colored noise induced by windowing [17]. The MAP and MLSE ICI equalizers [13], [15] offer the best bit-error rate (BER) performance, yet their cost is extremely high. Using the basis

Manuscript received February 17, 2012.
Manuscript revised June 26, 2012.

[†]The authors are with the Department of Electronics Engineering, National Chiao-Tung University, Hsin-Chu, Taiwan.
[††]The author is with the Mobile Device Corporation, Hsin-Chu, Taiwan.
a) E-mail: good.ee92g@nctu.edu.tw

DOI: 10.1587/transcom.E95.B.3509

expansion model [7], [13], [14] to develop ICI equalizers has been a hot research topic; however, its practical deployment is complicated by issues of channel estimation and model fitting. In short, there is a strong motivation to seek possible improvement on conventional ICI equalizers to strike a right balance between performance and implementation complexity.

In this paper, we focus on the inner receiver and develop low-complexity ICI equalizers for OFDMA downlink receivers. In Sect. 2, a popular model of linearly time-varying channel is reviewed and observations are made to serve as the inspiration of our approach. In Sect. 3, a per-subcarrier adaptive (PSA) ICI cancellation framework incorporating an ICI indicator, is introduced. With the PSA framework, it is possible to use different ICI cancellation strategies on different subcarriers according to the ICI situation, say, simple ICI cancellation for subcarriers experiencing mild ICI and heavy ICI cancellation for severe ICI. The PSA framework enables ICI equalizers achieve better trade-off between computational complexity and performance. In Sect. 4, novel low-complexity perturbation-based (PB) ZF and MMSE ICI equalizers are developed with the emphasis on implementation readiness and adequate performance. The proper mechanism of utilizing the ICI indicator is investigated to achieve robustness. Matrix inversion with lookup table (LUT) for subcarriers experiencing severe ICI is also developed to complement the PB ICI equalizers. In Sect. 5, through comprehensive simulations, results of BER performance and savings in computational cost verify the effectiveness of our approach. Finally, concluding remarks are given in Sect. 6.

2. Signal Model and ICI Structure

A variety of ICI signal models have been proposed in literatures. We choose a popular model that treats the channel variation within one OFDMA symbol as linear. This is a reasonable assumption for most scenarios in cellular systems currently in use. A sketch of the model is provided here for readers' convenience, while more details can be found in [5], [8]. Some crucial modifications and observations are also described to serve as the inspiration to develop our proposed PB-ZF and PB-MMSE ICI equalizers. Time-domain variables will be denoted by lowercase letters and frequency-domain variables by capital ones.

Consider the baseband equivalent OFDM system model with N subcarriers. The time-domain transmitted signal s_t at the tth time instant can be written as

$$s_t = \frac{1}{N}\sum_{m=0}^{N-1} S_m e^{\frac{j2\pi mt}{N}},\ t = 0, 1, \cdots, N-1 \tag{1}$$

where S_m are the modulated data on the mth subcarrier. Assume a cyclic prefix (CP) with length of N_{CP} longer than the maximum delay spread (L) of the channel; the total length of a transmitted OFDM symbol is $N_S = N + N_{CP}$. The time-domain received signal r_t is given by

$$r_t = \sum_{l=0}^{L-1} s_{t-l} h_{t,l} + z_t \tag{2}$$

where $h_{t,l}$ is the lth delay path of time varying channel impulse response (CIR) at tth time instant and z_t is the additive white Gaussian noise (AWGN). After removing CP and taking discrete Fourier transform (DFT), the frequency-domain received signal on the ith subcarrier is

$$\begin{aligned} R_i &= \sum_{t=0}^{N-1}\left(\sum_{l=0}^{L-1} s_{t-l} h_{t,l} + z_t\right) e^{\frac{-j2\pi ti}{N}} \\ &= \sum_{m=0}^{N-1} S_m H_{i,m} + Z_i \end{aligned} \tag{3}$$

where

$$H_{i,m} = \frac{1}{N}\sum_{t} H(m,t) e^{\frac{-j2\pi t(i-m)}{N}}. \tag{4}$$

and

$$H(m,t) = \sum_{l} h_{t,l} e^{\frac{-j2\pi lm}{N}} \tag{5}$$

Note that $H(m,t)$ can be interpreted as the CFR on the mth subcarrier at the tth time instant. ICI on the ith subcarrier which is caused by the signal on the mth transmit subcarrier comes through the ICI channel $H_{i,m}$.

Assume that the variation of CIR is a linear function in time domain, it an be written as

$$h_{nN_S-N+t,l} = h_{nN_S,l} - \frac{N-t}{N_S}\delta_{nN_S,l} \tag{6}$$

where $h_{nN_S-N+t,l}$ and $h_{nN_S,l}$ represent the lth path at $(n-1)$th and nth OFDM symbol, respectively, and $\delta_{nN_S,l}$ is the difference of CIR between the $(n-1)$th and the nth OFDM symbol. Substituting (6) into (5), we obtain

$$\begin{aligned} H(m, nN_S - N + t) &= \sum_{l}\left(h_{nN_S,l} - \frac{N-t}{N_S}\delta_{nN_S,l}\right) e^{\frac{-j2\pi lm}{N}} \\ &= H_m + \frac{t - \frac{N-1}{2}}{N_S}\Delta_m \end{aligned} \tag{7}$$

where H_m denotes the DFT of the CIR at the center time of the nth OFDM symbol:

$$H_m = \sum_{l}(h_{nN_S-\frac{N-1}{2},l}) e^{\frac{-j2\pi lm}{N}}, \tag{8}$$

and Δ_m is DFT of the CIR difference term,

$$\Delta_m = \sum_{l}\delta_{nN_S,l} e^{\frac{-j2\pi lm}{N}}. \tag{9}$$

From (7) it can be observed that the CFR on the mth subcarrier varies linearly. H_m can also be viewed as the average of the linearly varying frequency response.

Substituting (7) into (4), $H_{i,m}$ can be further decomposed as

$$H_{i,m} = \frac{1}{N}\sum_{t=0}^{N-1} H(m, nN_S - N + t)e^{\frac{-j2\pi t(i-m)}{N}} = H_m\xi_{i,m} + \Delta_m G_{i-m} \quad (10)$$

where $\xi_{i,m} = 1$ when $i = m$ and $\xi_{i,m} = 0$ otherwise; G_i accounts for the ICI:

$$G_i = \frac{1}{NN_S}\sum_{t=0}^{N-1}\left(t - \frac{N-1}{2}\right)e^{\frac{-j2\pi ti}{N}} \quad (11)$$

and can be approximated by

$$|G_i| \approx \frac{N}{2\pi N_S}\frac{1}{|i|},\ \angle G_i \approx -\frac{N+i}{2N}\pi. \quad (12)$$

Note that the approximation works well when the ratio $|i|/N$ is small. Fortunately, in practical systems such as WiMAX and LTE, the smallest number of subcarriers N is 128, and the approximation is accurate.

Defining $\mathbf{r} = [R_0, \ldots, R_{N-1}]^T$, $\mathbf{s} = [S_0, \ldots, S_{N-1}]^T$, and $\mathbf{z} = [Z_0, \ldots, Z_{N-1}]^T$, (3) and (10) can be compactly represented in the matrix form

$$\mathbf{r} = \mathbf{H}\mathbf{s} + \mathbf{z} \quad (13)$$

where the CFR matrix $\mathbf{H}$ can be decomposed as a combination of the averaged CFR matrix $\mathbf{H}_{avg}$ and the ICI matrix $\mathbf{G\Delta}$:

$$\mathbf{H} = \mathbf{H}_{avg} + \mathbf{G\Delta} = \begin{pmatrix} H_0 & 0 & \cdots & 0 \\ 0 & H_1 & & \vdots \\ \vdots & & \ddots & 0 \\ 0 & \cdots & 0 & H_{N-1} \end{pmatrix} + \begin{pmatrix} 0 & G_{-1} & \cdots & G_{-(N-1)} \\ G_1 & 0 & & \vdots \\ \vdots & & \ddots & G_{-1} \\ G_{N-1} & \cdots & G_1 & 0 \end{pmatrix}\begin{pmatrix} \Delta_0 & 0 & \cdots & 0 \\ 0 & \Delta_1 & & \vdots \\ \vdots & & \ddots & 0 \\ 0 & \cdots & 0 & \Delta_{N-1} \end{pmatrix}. \quad (14)$$

Substitute (14) into (13), we have

$$\mathbf{r} = \mathbf{H}_{avg}\mathbf{s} + \mathbf{G\Delta s} + \mathbf{z}. \quad (15)$$

A crucial detail in (15) is observed. Note that the diagonal matrix $\mathbf{\Delta}$ multiplies $\mathbf{G}$ from the right; it means that the column vectors of the ICI matrix are weighted by different Δ_i. Each column vector registers how a signal on the corresponding subcarrier is spread over and affects other subcarriers. Therefore, different weights mean that the spreading effect is different from subcarrier to subcarrier. We can rearrange (15) into another form:

$$\underbrace{(\mathbf{\Delta H}_{avg}^{-1})\mathbf{r}}_{\tilde{\mathbf{r}}} = \underbrace{[\mathbf{I}_N + (\mathbf{\Delta H}_{avg}^{-1})\mathbf{G}]}_{\tilde{\mathbf{H}}}\underbrace{(\mathbf{\Delta s})}_{\tilde{\mathbf{s}}} + \underbrace{(\mathbf{\Delta H}_{avg}^{-1})\mathbf{z}}_{\tilde{\mathbf{z}}} \quad (16)$$

where $\mathbf{I}_N$ denotes the $N \times N$ identity matrix and $\mathbf{G}$ is multiplied by the diagonal matrix $(\mathbf{\Delta H}_{avg}^{-1})$ from the left; this time, the k-th row vector of the ICI matrix is weighted by a corresponding (Δ_k/H_k), which registers how much the k-th subcarrier is affected by its neighboring subcarriers. That is, (Δ_k/H_k) indicates the ICI level experienced by the k-th subcarrier. This rearrangement allows the development of the ICI indicator and the low-complexity ICI equalizers described later.

3. The Per-Subcarrier Adaptive ICI Cancellation Framework

As mentioned in Introduction, a common means to reduce the complexity of ICI equalization is to approximate the non-diagonal CFR matrix with a banded matrix. For example, the approximation by banded CFR matrices can be utilized to construct the so-called *block* and *serial* ICI equalizers [9]. The CFR matrix $\mathbf{H}$ in (13) is first approximated by a banded matrix $\mathbf{B}$ in which all but few elements on the selected $2Q + 1$ diagonals are set to zero. The transmitted signal $\mathbf{s}$ can be estimated by solving the resulted linear model, either by ZF or MMSE criteria. Figure 2 illustrates the difference between the block and serial approaches. In the block approach, the whole system of linear equations is solved altogether, e.g, the banded matrix $\mathbf{B}$ is directly inverted in the ZF approach to find the estimation of $\mathbf{s}$. While in the serial approach, for each subcarrier a local $(2Q + 1) \times (2Q + 1)$ banded CFR matrix is considered, i.e., consider $\mathbf{B}_k^{(Q)} \triangleq [\mathbf{H}]_{\{<k-Q:k+Q>_N, <k-Q:k+Q>_N\}}$ (note that $\langle\cdot\rangle_N$ means the modulo-N operation), and a truncated $(2Q + 1) \times (2Q + 1)$ system of linear equations is solved for each subcarrier. Apparently, the serial approach enjoys an even lower complexity than the block approach does, but it also results in a larger performance degradation since the truncation in building smaller systems of linear equations introduces larger approximation errors.

The approach of using banded CFR matrices is, how-

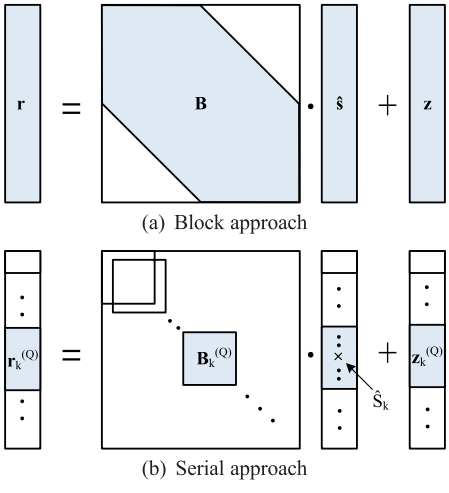

Fig. 2 Block and serial approaches for ICI equalization.

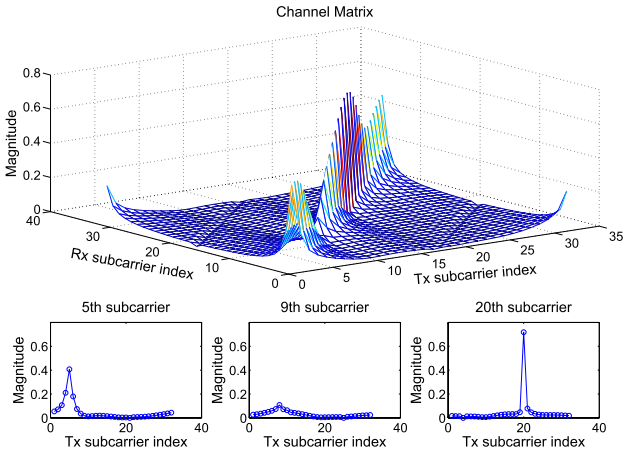

Fig. 3 The magnitude of the CFR matrix and cross-sections at selected subcarriers.

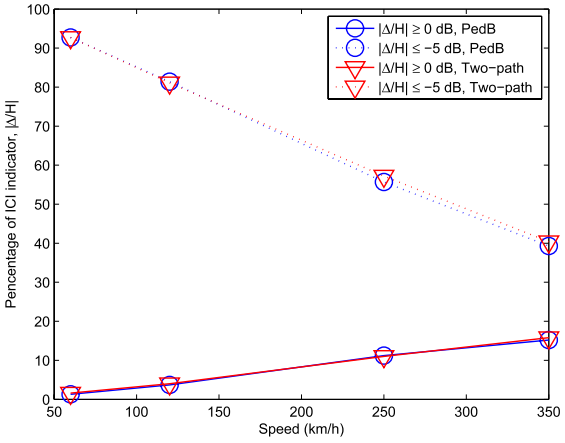

Fig. 4 The percentages of $|\Delta_k/H_k|$ that are larger than 0 dB or smaller than −5 dB at different vehicle speeds. Two channel PDPs, the ITU Pedestrian-B channel and the two-path equal-gain channel, are used.

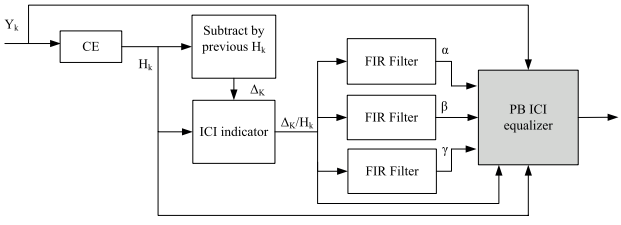

Fig. 5 A receiver adopting the PSA framework.

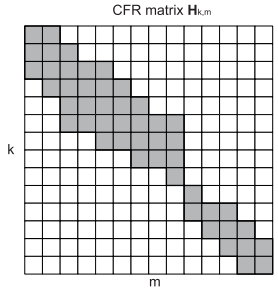

Fig. 6 A banded CFR matrix with variable bandwidth Q.

ever, highly inefficient, especially taking into account the fact that each subcarrier can experience vastly different ICI scenarios. Intuitively, if different counter-ICI measures are adopted for different subcarrier, possible benefits of reduced complexity and/or enhanced performance may follow. A closer look at the ICI model in (15) and (16) provides details about the different ICI scenarios faced by each subcarrier. Figure 3 shows the magnitude of a 32×32 example CFR matrix and three cross-sections on three subcarriers. It is clear that a uniform banded approximation is inappropriate, since each subcarrier faces very different ICI situations. Inspired by the observations made from (16), a metric $|\Delta_k/H_k|$, is introduced to indicate the ICI severity on the kth subcarrier. Given the value of $|\Delta_k/H_k|$, the signal-to-interference ratio (SIR) can be easily calculated from (15). In Fig. 3, the 20th subcarrier, with a small $|\Delta_k/H_k|$ ($|\Delta_k/H_k| < -5$ dB, SIR > 22 dB), is affected by insignificant amount of ICI. When moderate fading occurs, like on the 5th subcarrier, $|\Delta_k/H_k|$ becomes higher, and moderate ICI emerges. When deep fading occurs, as on the 9th subcarrier, $|\Delta_k/H_k|$ becomes significant ($|\Delta_k/H_k| > 0$ dB, SIR < 12 dB), severe ICI exists and heavy ICI cancellation may be needed to maintain BER performance. The term $|\Delta_k/H_k|$ is able to indicate the ICI situation and the different need of ICI cancellation strategies on each subcarrier.

Our experiences show that in practical situations, the majority of subcarriers face moderate or very mild ICI situations; that is, little or no ICI cancellation needs to be done on these subcarriers and the performance will not suffer. Figure 4 gives an idea of how many percentages of subcarriers face very mild ($|\Delta_k/H_k| < -5$ dB) and heavy ICI ($|\Delta_k/H_k| > 0$ dB). The simulation is conducted under WiMAX standard: 10 MHz bandwidth, 2.5 GHz central frequency, and 1024 subcarriers. Two very different channel power delay profiles (PDPs) are considered: the ITU Pedestrian-B (PedB) channel and a two-path equal-gain channel. Different vehicle speeds from 60 km/h to the maximum speed of 350 km/h suggested in the LTE and WiMAX standards are simulated. The results show that as vehicle speed gets higher, more subcarriers experience severe ICI; yet even at 350 km/h, there are still 85% of subcarriers on which $|\Delta_k/H_k| < 0$ dB. An interesting observation is that the percentages of the ICI indicator remain almost the same when the channel PDP changes; therefore we expect the ICI indicator work properly for different types of channels.

Based on the ICI indicator, a PSA receiver architecture shown in Fig. 5 is proposed. A variety of existing ICI equalizers can be incorporated into this architecture and their settings can be adapted on each subcarrier according to $|\Delta_k/H_k|$; in this way, a better trade-off between computational complexity and performance can be achieved. PSA utilizes the idea of using different Q on each subcarrier to approximate the CFR matrix $\mathbf{H}$. Figure 6 depicts how the CFR matrix $\mathbf{H}$, instead of being approximated by a banded matrix with fixed bandwidth Q as shown in Fig. 2, is approx-

imated by a banded matrix with variable bandwidth adaptively set at each subcarrier. The approach also works well with popular wireless access technologies such as WiMAX and LTE based on OFDMA. In the following section, the PSA architecture forms the foundation for us to develop novel low-complexity ICI methods with remarkable results.

In practice, the ICI indicator is obtained as the ratio between the estimates of Δ_k and H_k. An estimation method that uses consecutive OFDM symbols is provided in [8]. Here, with the goal of keeping complexity low, a simpler method is used. Instead of estimating the complete ICI model as in [8], we use the estimate of the averaged CFR, $\hat{H}_k$, which is always needed for signal demodulation. The estimate of Δ_k is simply obtained as the difference between $\hat{H}_k$ of adjacent OFDMA symbols due to the fact that CFR varies linearly across time-domain:

$$\hat{\Delta}_k^{(n)} = \hat{H}_k^{(n)} - \hat{H}_k^{(n-1)}$$

where superscript (n) denotes the symbol index. Though the estimate is not very accurate, the degradation in simulated BER performance is insignificant. Advanced channel estimation techniques for time-varying channels may also be used [2]–[5], [16], but we regard this as unnecessary in the current setting.

4. Proposed Novel Low-Complexity ICI Equalizers

4.1 Perturbation-Based ZF ICI Equalizer

The PSA architecture allows different strategies be adopted for each subcarrier according to the ICI indicator. For subcarriers inflicted by severe ICI, costly methods, say, matrix inversion, are needed; while for subcarriers inflicted by mild ICI, very simple equalizers suffice to provide good performance. In this subsection, simple perturbation-based (PB) equalizers that are perfect for treating mild ICI are developed. Figure 7 shows the block diagram of the proposed PB ICI equalizers.

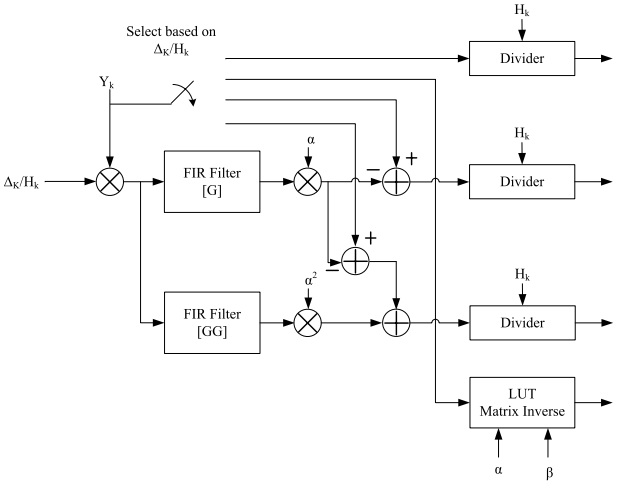

Fig. 7 PB ICI equalizer block diagram.

Start with (16) and zoom in the neighboring $2Q + 1$ subcarriers of the kth subcarrier. The superscript (Q) and subscript k will be dropped temporarily for simplicity. A serial ZF equalizer on the kth subcarrier operates as follows

$$\begin{aligned}\hat{S}_k &= \mathbf{wr} = \mathbf{e}_c\boldsymbol{\Delta}^{-1}\tilde{\mathbf{H}}^{-1}(\boldsymbol{\Delta}\mathbf{H}_{avg}^{-1})\mathbf{r} \\ &= \mathbf{e}_c\boldsymbol{\Delta}^{-1}(\mathbf{I}_{2Q+1} + (\boldsymbol{\Delta}\mathbf{H}_{avg}^{-1})\mathbf{G})^{-1}(\boldsymbol{\Delta}\mathbf{H}_{avg}^{-1})\mathbf{r}, \end{aligned} \tag{17}$$

where the $1 \times (2Q + 1)$ row vector $\mathbf{w}$ denotes the equalizer and $\mathbf{e}_c$ is a $1 \times (2Q + 1)$ row vector with 1 at the center and zeros elsewhere. The diagonal matrix $(\boldsymbol{\Delta}\mathbf{H}_{avg}^{-1})$ will be approximated by a model with few parameters. The goals are two-folded: a simple model makes it possible to replace $\mathbf{w}$ with simple filters on subcarriers facing mild ICI; meanwhile the matrix inversion $(\mathbf{I}_{2Q+1} + (\boldsymbol{\Delta}\mathbf{H}_{avg}^{-1})\mathbf{G})^{-1}$ is available to fight severe ICI, with the corresponding inverse matrices being calculated off-line and stored in a LUT indexed by the parameters α, β and γ in (18).

Polynomial curve fitting is used to approximate the local CFR fluctuation of $(\boldsymbol{\Delta}\mathbf{H}_{avg}^{-1})$:

$$(\boldsymbol{\Delta}\mathbf{H}_{avg}^{-1}) \approx \alpha\mathbf{I}_{2Q+1} + \beta\mathbf{L} + \gamma\mathbf{P} \tag{18}$$

where $\mathbf{L}$ and $\mathbf{P}$ are both diagonal with linear and parabolic shapes, i.e., $\mathbf{L} = \text{diag}(Q, Q-1, \ldots, -Q)$ and $\mathbf{P} = \text{diag}(Q^2, (Q-1)^2, \ldots, (-Q)^2)$. Substituting (18) into (17) and applying $(\mathbf{I} + \mathbf{A})^{-1} \approx \mathbf{I} - \mathbf{A} + \mathbf{A}^2 + o(\epsilon)$ where $\mathbf{A}$ is the perturbation term and $o(\epsilon)$ denotes the higher-order terms, the low-complexity ICI equalizer can be obtained. Ignoring high-order terms, the first-order PB-ZF equalizer is given by

$$\mathbf{w}_{ZF^{1st}} = \mathbf{e}_c\mathbf{H}_{avg}^{-1} - \frac{1}{\Delta_k}(\alpha\mathbf{e}_c\mathbf{G})(\boldsymbol{\Delta}\mathbf{H}_{avg}^{-1}). \tag{19}$$

Including second-order terms gives the second-order PB-ZF equalizer:

$$\mathbf{w}_{ZF^{2nd}} = \mathbf{e}_c\mathbf{H}_{avg}^{-1} - \frac{1}{\Delta_k}(\alpha\mathbf{e}_c\mathbf{G} - \alpha^2\mathbf{e}_c\mathbf{G}^2)(\boldsymbol{\Delta}\mathbf{H}_{avg}^{-1}). \tag{20}$$

Two approximations are involved here: the approximation of $(\boldsymbol{\Delta}\mathbf{H}_{avg}^{-1})$ and the approximation of $(\mathbf{I}_{2Q+1} + (\boldsymbol{\Delta}\mathbf{H}_{avg}^{-1})\mathbf{G})^{-1}$. In most cases ZF equalizers with only lower-order terms are good enough. When ICI is severe, more costly methods (matrix inversion, for example) involved with β and γ may be used.

A crucial advantage of our approach becomes clear by observing that, without the approximation in (18), the conventional perturbation method that uses $(\mathbf{I} + \mathbf{A})^{-1} \approx \mathbf{I} - \mathbf{A} + \mathbf{A}^2 + o(\epsilon)$ will yield

$$\begin{aligned}\mathbf{w}_{ZF^{2nd}} &= \mathbf{e}_c\mathbf{H}_{avg}^{-1} - \mathbf{e}_c\mathbf{H}_{avg}^{-1}(\mathbf{G}\boldsymbol{\Delta}\mathbf{H}_{avg}^{-1}) \\ &\quad + \mathbf{e}_c\mathbf{H}_{avg}^{-1}\mathbf{G}(\boldsymbol{\Delta}\mathbf{H}_{avg}^{-1})\mathbf{G}(\boldsymbol{\Delta}\mathbf{H}_{avg}^{-1}). \end{aligned} \tag{21}$$

In this case, the matrix multiplications within the second term of (21) $\mathbf{e}_c\mathbf{H}_{avg}^{-1}\mathbf{G}(\boldsymbol{\Delta}\mathbf{H}_{avg}^{-1})\mathbf{G}(\boldsymbol{\Delta}\mathbf{H}_{avg}^{-1})$ cannot commute. That is, the signal will be multiplied by $(\boldsymbol{\Delta}\mathbf{H}_{avg}^{-1})$, filtered by $\mathbf{G}$, then multiplied by $(\boldsymbol{\Delta}\mathbf{H}_{avg}^{-1})$ before getting filtered by $\mathbf{G}$

again. Our approximation results in a more efficient filtering procedure. With the polynomial approximation of $(\mathbf{\Delta H}_{avg}^{-1})$, the proposed perturbation equalization in (20) mainly consists of fixed finite-impulse response (FIR) filters, i.e., the central row vectors of $\mathbf{G}$ and $(\mathbf{GG})$.

When the ICI is severe, matrix inversion may be needed to achieve decent ICI cancellation. By extracting the parameters $\{\alpha, \beta, \gamma\}$, a LUT of matrix inversion indexed by $\{\alpha, \beta, \gamma\}$ can be pre-calculated off-line and applied when needed. The LUT of matrix inversion will be described in more details in Sect. 4.4.

4.2 Perturbation-Based MMSE ICI Equalizer

When a channel goes into a fade, MMSE equalizers are more effective than ZF equalizers in preventing noise enhancement. In order to take advantage of the re-arrangement in (16) for developing low-complexity filters, the MMSE solution of $\tilde{\mathbf{s}}$ instead of $\mathbf{s}$ is derived, and the inverse mapping $\mathbf{\Delta}^{-1}\tilde{\mathbf{s}}$ is used to recover $\mathbf{s}$. Strictly speaking, this procedure differs from conventional MMSE approaches because the noise term $(\mathbf{\Delta H}_{avg}^{-1})\mathbf{z}$ has different power levels on each subcarrier. But the effect on performance is negligible, due to reasons explained next. Consider serial equalizers, the corresponding channel matrix for each subcarrier is a truncated matrix, that is, a $(2Q+1)\times(2Q+1)$ one within which the noise is treated as white with a localized SNR. For practical channel scenarios, computer simulations show that this assumption of whiteness is quite accurate and has little impact on performance. Therefore, locally white noise with a localized SNR is assumed for the development of PB-MMSE ICI equalizers.

A typical MMSE IC equalizer is:

$$\begin{aligned}\mathbf{w} &= \mathbf{e}_c\mathbf{\Delta}^{-1}\tilde{\mathbf{H}}^*\left[\tilde{\mathbf{H}}\tilde{\mathbf{H}}^* + \frac{1}{\rho_k}\mathbf{I}\right]^{-1}(\mathbf{\Delta H}_{avg}^{-1}) \\ &= \mathbf{e}_c\mathbf{\Delta}^{-1}(\mathbf{I}+(\mathbf{\Delta H}_{avg}^{-1})\mathbf{G})^*\times \\ &\quad\left[(\mathbf{I}+(\mathbf{\Delta H}_{avg}^{-1})\mathbf{G})(\mathbf{I}+(\mathbf{\Delta H}_{avg}^{-1}\mathbf{G}))^* + \frac{1}{\rho_k}\mathbf{I}\right]^{-1}(\mathbf{\Delta H}_{avg}^{-1})\end{aligned} \tag{22}$$

where * denotes the complex conjugate transposition and ρ_k the *localized* SNR which is estimated from $2Q+1$ neighboring subcarriers.

By applying the polynomial approximation of $(\mathbf{\Delta H}_{avg}^{-1})$ and the perturbation approximation of $(\mathbf{I}+\mathbf{A})^{-1}$ where $\mathbf{A}$ is the perturbation term, the PB-MMSE ICI equalizer is obtained. When the localized SNR on a subcarrier is large, higher order terms can be ignored, and we have the first-order PB-MMSE ICI equalizer:

$$\begin{aligned}\mathbf{w}_{MMSE^{1st}} &= \frac{\rho}{\rho+1}\mathbf{e}_c\mathbf{H}_{avg}^{-1} - \frac{1}{\Delta_k}\cdot\frac{\rho}{\rho+1} \\ &\quad\times\left[\frac{\rho}{\rho+1}\alpha\mathbf{e}_c\mathbf{G} + \frac{1}{\rho+1}\alpha^*\mathbf{e}_c\mathbf{G}^*\right. \\ &\quad\left.+\frac{1}{\rho+1}\beta^*\mathbf{e}_c\mathbf{G}^*\mathbf{L}^* + \frac{1}{\rho+1}\gamma^*\mathbf{e}_c\mathbf{G}^*\mathbf{P}^*\right](\mathbf{\Delta H}_{avg}^{-1}).\end{aligned} \tag{23}$$

If $\mathbf{H}_{avg}$ is close to a fade, higher-order terms with α^2 are added, and the second-order PB-MMSE ICI equalizer is:

$$\begin{aligned}&\mathbf{w}_{MMSE^{2nd}} = \frac{\rho}{\rho+1}\mathbf{e}_c\mathbf{H}_{avg}^{-1} - \frac{1}{\Delta_k}\cdot\frac{\rho}{\rho+1} \\ &\times\left[\frac{\rho}{\rho+1}\alpha\mathbf{e}_c\mathbf{G} + \frac{1}{\rho+1}\alpha^*\mathbf{e}_c\mathbf{G}^* + \frac{1}{\rho+1}\beta^*\mathbf{e}_c\mathbf{G}^*\mathbf{L}^*\right. \\ &+ \frac{1}{\rho+1}\gamma^*\mathbf{e}_c\mathbf{G}^*\mathbf{P}^* - \frac{\rho^2}{(\rho+1)^2}\alpha^2\mathbf{e}_c\mathbf{G}^2 \\ &\left.+ \frac{\rho}{(\rho+1)^2}(\alpha^*)^2\mathbf{e}_c\mathbf{G}^*\mathbf{G}^* + \frac{2\rho}{(\rho+1)^2}|\alpha|^2\mathbf{e}_c\mathrm{Re}(\mathbf{G}^*\mathbf{G})\right](\mathbf{\Delta H}_{avg}^{-1}).\end{aligned} \tag{24}$$

Note that the row vectors $\mathbf{e}_c\mathbf{LG}$ and $\mathbf{e}_c\mathbf{PG}$ are zero vectors and discarded in the derivations.

4.3 ICI Indicator Threshold Setting

Since the PSA framework relies on the ICI indicator $|\Delta_k/H_k|$ to determine which ICI cancellation methods to use for each subcarrier, it is crucial to determine the thresholds against which the PSA framework compares the ICI indicator. The thresholds should be chosen for the PSA framework to operate robustly for a wide range of SNR. It can be done by comprehensive simulations. Define the residual interference plus noise at the ICI equalizer output as

$$\varepsilon_k = S_k - \hat{S}_k = S_k - \mathbf{w}_k\mathbf{r}_k. \tag{25}$$

The post-detection SINR at the ICI equalizer output is defined as $\mathrm{SINR}_{post} = \mathrm{E}[\|\mathbf{H}_{avg}\mathbf{s}\|^2/\|\boldsymbol{\varepsilon}\|^2]$ where $\boldsymbol{\varepsilon} = [\varepsilon_0, \ldots, \varepsilon_{N-1}]^T$. The approximate symbol error rate (SER) expression for rectangular M-QAM is

$$P_{SER} = 2\left(1-\frac{1}{\sqrt{M}}\right)Q\left(\sqrt{\frac{3}{M-1}\mathrm{SINR}_{post}}\right) \tag{26}$$

where $Q(x) = \frac{1}{\sqrt{2\pi}}\int_x^\infty e^{-\frac{u^2}{2}}du$.

With extensive simulations on SER for various SNRs and velocities, proper ICI indicator thresholds can be found by looking at when higher-order equalizers begin to provide performance benefits. A proper threshold setting should not deviate much from these observed forking points for a wide range of SNRs. With the same simulation setting as that in Sect. 3, Fig. 8 shows SER of PB-ZF ICI equalizers versus $|\Delta_k/H_k|$ at 350 km/h under 10, 20 and 30 dB SNR, respectively. It can be seen that when SNR is low, AWGN dominates and all ICI equalizers provide no significant benefits

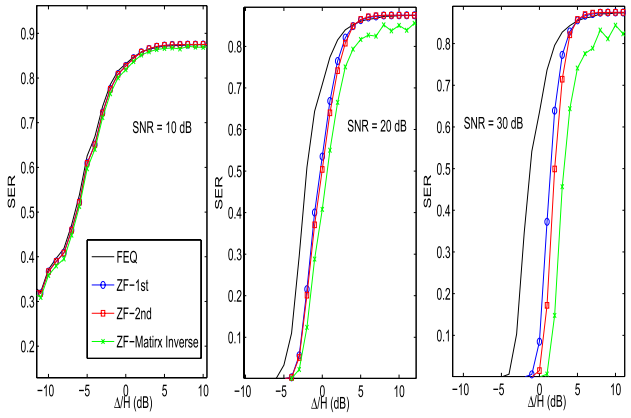

Fig. 8 SER performance versus $|\Delta_k/H_k|$ at 10, 20 and 30 dB SNR.

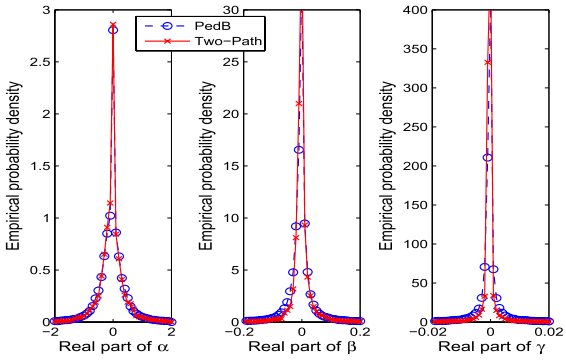

Fig. 9 Empirical probability density functions of α, β and γ for two different channel PDPs: the ITU Pedestrian-B channel and a two-path equal-gain channel.

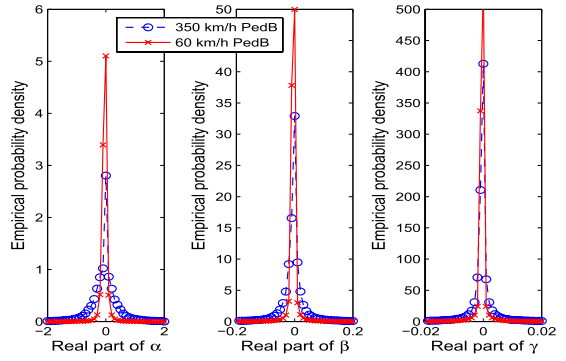

Fig. 10 Empirical probability density functions of α, β and γ for the ITU Pedestrian-B channel at two different vehicle speeds: 350 km/h and 60 km/h.

compared to conventional one-tap frequency domain equalizer (FEQ). When SNR becomes larger, the first-order PB-ZF ICI equalizer begins to outperform one-tap FEQ when $|\Delta_k/H_k| > -6$ dB and the second-order PB-ZF ICI equalizer excels the first-order one when $|\Delta_k/H_k| > -3$ dB. ZF Matrix Inversion outperforms the perturbation-based methods when $|\Delta_k/H_k| > 0$ dB. The threshold settings for PB-MMSE ICI equalizers can also be investigated in a similar way.

Note that the BER floor due to ICI starts to kick in around SNR = 20 dB and thus an appropriate threshold setting may be between -20 and -30 dB target residual ICI power. Furthermore, with a additional 3-dB margin, the threshold setting that four ranges (≤ -5 dB, $-5 \sim -3$ dB, $-3 \sim 0$ dB, and ≥ 0 dB) of $|\Delta_k/H_k|$ is a good choice for many realistic situations and adopted in the later simulations.

4.4 CFR Matrix Inversion by Lookup Table

When the subcarrier experiences severe ICI, the approximate matrix inverse $\mathbf{I} - \mathbf{A} + \mathbf{A}^2 + \cdots + \mathbf{A}^p$ adopted in PB-ZF and PB-MMSE ICI equalizers become a crude approximation and the error rate performance may degrade significantly. Hence, the exact matrix inverse, $(\mathbf{I} + \mathbf{A})^{-1}$, which demands high computational load is needed. Though the PB method is no longer appropriate, the localized CFR matrix approximated by polynomial functions as (18) is still accurate enough for the matrix inversion. We propose an LUT in which pre-calculated matrix inverses indexed by quantized parameters α, β and γ are stored and can be applied on the fly. The computational cost of matrix inverse is $O(N^3)$ while the cost is reduced to $O(N)$ by adopting the LUT approach.

In practice, a trade-off between the number of quantization levels and the corresponding quantization error should be carefully designed to avoid performance degradation. By comprehensive computer simulations, the empirical probability density functions (PDFs) of α, β and γ for different channel PDPs at 350 km/h and for the ITU Pedestrian-B channel at different vehicle speeds are shown in Figs. 9 and 10 respectively. The empirical PDFs, like the ICI indicator, are insensitive to changes in channel PDPs. Furthermore, the empirical PDFs are quite concentrated; in fact, the lower the vehicle speed, the more concentrated they are. As a result, eight equally-spaced levels spanning from -2 to 2 is enough for quantizing α. Similarly, eight levels are used for quantizing β and γ. The total number of matrix inverses to be stored is 4096. For each matrix inverse, we only need to store the central row because the serial ICI equalizer is considered. For 12-bit fixed-point numerical resolution, the LUT size will be 16 KBytes. The detailed simulation results concerning the trade-off between BER performance and quantization levels will be provided in Sect. 5.1.

It is worth noting that an LUT can always be used when matrix inversion is needed. However, without our transposed signal model in (16), the LUT approach will not be effective. For example, an LUT of matrix inversion for the signal model in (15) needs to parameterize $\mathbf{H}_{avg}$ and $\mathbf{\Delta}$ in $[\mathbf{H}_{avg} + \mathbf{G}\mathbf{\Delta}]^{-1}$. There will be two sets of parameters and two dynamic ranges to consider. Consequently, the resulted LUT will be too large to be effective.

5. Performance

5.1 BER Simulations

In this subsection, we investigate the performance and robustness of proposed ICI equalizers under different system

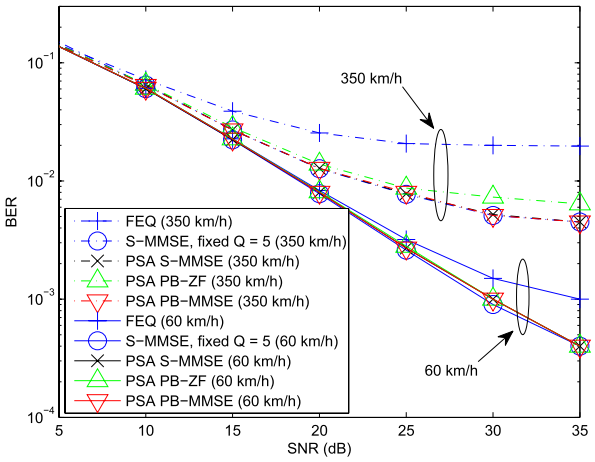

Fig. 11 BER performance comparisons for ICI equalizers under 1024-point FFT, 16-QAM and the ITU Pedestrian-B channel model at 350 km/h and 60 km/h.

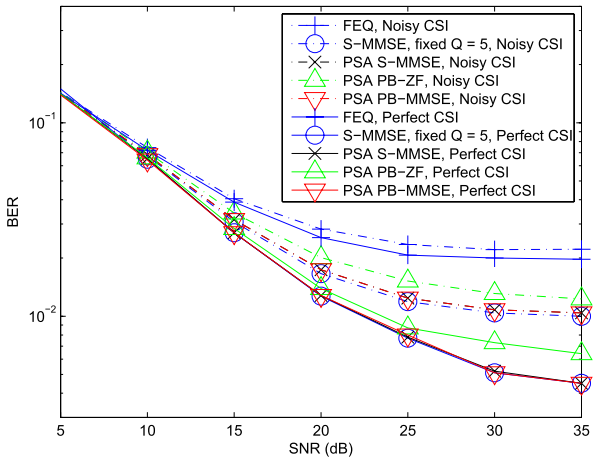

Fig. 12 BER performance comparisons with −20 dB MSE channel estimation error at 350 km/h.

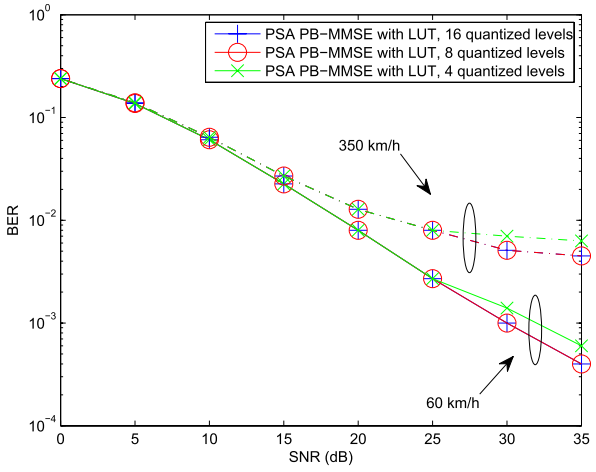

Fig. 13 BER with different quantization levels LUT under the ITU Pedestrian-B channel at 350 and 60 km/h.

parameters and channel conditions. Unless otherwise stated, perfect channel state information (CSI) of the averaged CFR (H_k) is assumed. The ICI CFR, Δ_k, and the ICI indicator are estimated by the simple method mentioned in Sect. 3. First, with the same simulation set-up described in Sect. 3 with $N_A = 840$ active subcarriers, BER curves of different ICI equalizers at 60 km/h and 350 km/h are shown in Fig. 11. The serial MMSE (S-MMSE) ICI equalizer inverts for each subcarrier a local CFR sub-matrix whose size is $(2Q + 1) \times (2Q + 1)$ fixed for all subcarriers. The PSA ICI equalizers adjust Q according to the ICI indicator and the corresponding threshold setting is described in Sect. 4.3. In Fig. 11, the PSA S-MMSE ICI equalizer with $Q \leq 5$ achieves, with lower complexity, the same BER as the conventional S-MMSE ICI equalizer with fixed $Q = 5$. Moreover, our PSA PB-MMSE ICI equalizers provide further complexity reduction without BER degradation, compared to the PSA S-MMSE ICI equalizers. Note that PB-ZF ICI equalizer suffers slightly performance degradation due to the noise enhancement effect. The results verify the effectiveness of the PSA PB ICI equalizers to improve the balance between performance and computational complexity. The results also indicate that the PSA approach is effective for different vehicle speeds. Intuitively this is expected, because the idea of PSA is to adjust the complexity of the ICI equalizer according to the ICI indicator, and the ICI indicator works fine regardless what the vehicle speed is. Moreover, as can be seen from Fig. 8, simple methods such as one-tap FEQ perform as good as sophisticated equalizers when $|\Delta_k/H_k|$ indicates little ICI. We conclude that the PSA approach works effectively for different vehicle speeds.

The impact due to the channel estimation error is also considered. Figure 12 shows the results under imperfect CSI. Follow the practice found in [16], [17], the mean-square error (MSE) of the channel estimation is set to −20 dB. The accuracy of channel estimation will effect the performance of any ICI cancellation methods. As for our method, there are two aspects that deserve discussion. The first is that it is built on a linear approximation of time-varying channels; therefore, it only requires estimating the averaged channel response, which is routinely done by OFDMA receivers in block-fading channels. The second is that, though the performance degradation is inevitable, our method is effected in a comparable way by which other linear methods, say, conventional S-MMSE ICI equalizers, are effected.

Next, we study how many quantization levels in LUT are enough for the PB ICI equalizers. From Fig. 13, it can be seen that an 8-levels LUT has the same BER performance as a 16-level LUT, but a 4-level LUT will result in performance degradation. Consequently, an 8-level LUT is chosen for 350 km/h, i.e., the worst-case scenario, to make sure that it is enough for all speeds.

Finally, we consider the coded performance and compare the packet error rate (PER) of different ICI equalizers in Fig. 14. The modulation is 16-QAM and the channel coding is a rate-3/4 convolutional turbo code (CTC) that is mandatory in WiMAX [1]. Ten iterations of CTC decoding

Table 1 Complexity comparison.

Methods	Complexity	Number of complex flops
Ideal B-MMSE	$O(N_A^3)$	4×10^8
Conventional fixed Q S-MMSE	$O(Q^3 N_A)$	745360($Q = 5$) / 408240($Q = 4$) / 192080($Q = 3$)
PSA Variable $Q \le 5$ S-MMSE	$\sum_i O(Q_i^3 N_A)$	162334 (350 km/h) / 14301 (60 km/h)
PSA PB-ZF with LUT	$O(QN_A)$	68388 (350 km/h) / 6822 (60 km/h)
PSA PB-MMSE with LUT	$O(QN_A)$	93883 (350 km/h) / 10340 (60 km/h)

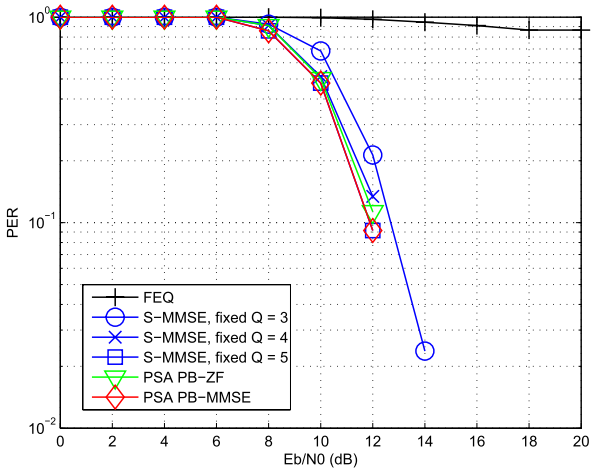

Fig. 14 PER comparison for different Q = 3, 4 and 5 under the ITU Pedestrian-B channel at 350 km/h. 16-QAM and rate-3/4 CTC are used.

are conducted. Under this configuration, one packet consists of 44 bytes payload. The standard requires 10% PER at 12 dB Eb/N0 [18] where Eb/N0 is defined as the SNR per bit. From Fig. 14, it can be seen that at 350 km/h the performances of linear equalizers are close to borderline. The S-MMSE with fixed $Q = 5$ and our PSA PB-MMSE offer the best performances with a very tight margin to spare. This demonstrates the value of our approach. The PSA equalizer can opt for a higher upper limit on Q with a reasonable increase in complexity, if a larger performance margin is required. But for a fixed-Q equalizer, the option to increase Q may be not feasible.

5.2 Computational Complexity

The computational complexity is measured in complex floating point operations (flops) and summarized in Table 1. The reduction of computational cost by our PSA framework incorporating PB-ZF/PB-MMSE equalizers and matrix inversion with LUT is shown. The calculation of equalizer coefficients dominates the computational cost. The ideal Block MMSE (B-MMSE) ICI equalizer inverts the whole $N_A \times N_A$ CFR matrix and requires $2{N_A}^3/3 \approx 4 \times 10^8$ flops which is unaffordably high, and the conventional S-MMSE ICI equalizer needs about $2(2Q+1)^3 N_A/3 \approx 7.5 \times 10^5$ flops with $Q = 5$. They are used as benchmarks for comparison.

We then consider the complexity of proposed PSA approaches. Notice that the complexity of calculation of the ICI indicator is one complex division per subcarrier and has been included in Table 1. Define Q_i as the value of Q chosen in the i-th $|\Delta_k/H_k|$ range and N_i as the number of subcarriers in that range. For example, in PSA S-MMSE equalizers, at the first stage ($Q_1 = 0$), there are $N_1 = 0.393N_A$ of subcarriers that use one-tap FEQ and, at the last stage ($Q_4 = 5$), there are $N_4 = 0.152N_A$ of subcarriers that use 11×11 matrix inversion resulting in the complexity of $O(Q_4^3 N_4)$. Overall, its complexity is $\sum_{i=1}^{4} O(Q_i^3 N_i)$, which leads to 1.6×10^5 flops at 350 km/h, about 4.5 times lower than that of the banded S-MMSE with fixed $Q = 5$.

The PSA PB-ZF and PB-MMSE ICI equalizers achieve big savings with their complexity in $O(QN_A)$. In practice, PB-ZF and PB-MMSE ICI equalizers are used for subcarriers inflicted by mild ICI, while the LUT matrix inversion is used to combat severe ICI. For each subcarrier, the first-order PB-ZF requires $8Q + 7$ flops and the second-order PB-ZF requires $12Q + 12$ flops due to one and two Q-tap fixed FIR filters, respectively. Similarly, the first-order PB-MMSE requires $28Q + 23$ flops and the second-order PB-MMSE requires $36Q + 31$ flops. Overall, the complexity of PB-ZF and PB-MMSE with LUT matrix inversion are about 11 and 8 times lower than that of the conventional S-MMSE equalizer with fixed $Q = 5$ at 350 km/h. Furthermore, it can be seen that the save in complexity is also prominent at lower speed, say, 60 km/h.

6. Conclusions

In this paper, perturbation-based zero-forcing and minimum mean-square error ICI equalizers with very low complexity are developed within the per-subcarrier adaptive (PSA) processing framework incorporating an ICI indicator. They are very effective at dealing with mild ICI situations. A lookup table method is also developed that forms, together with these equalizers, a comprehensive ICI solution for OFDMA downlink receivers. Theoretical analysis and simulations are provided to show the effectiveness of our approach.

Acknowledgment

The authors thank Prof. David W. Lin for his careful reading and insightful suggestions. This work was supported in part by the National Science Council of R.O.C. under Grants NSC 100-2220-E-009-003 and NSC 100-2220-E-009-063.

References

[1] Draft IEEE Standard for Local and Metropolitan Area Networks Part 16: Air Interface for Fixed and Mobile Broadband Wireless Access Systems, IEEE P802.16e/D7, 2005.
[2] W.G. Jeon, K.H. Chang, and Y.S. Cho, "An equalization technique for orthogonal frequency-division multiplexing systems in time-variant multipath fading channels," IEEE Trans. Commun., vol.47, no.1, pp.27–32, Jan. 1999.
[3] A. Stamoulis, S.N. Diggavi, and N. Al-Dhahir, "Intercarrier interference in MIMO OFDM," IEEE Trans. Signal Process., vol.50, no.10, pp.2451–2464, Oct. 2002.
[4] X. Cai and G.B. Giannakis, "Bounding performance and suppressing intercarrier interference in wireless mobile OFDM," IEEE Trans. Commun., vol.51, no.12, pp.2047–2056, Dec. 2003.
[5] A. Gorokhov and J.P. Linnartz, "Robust OFDM receivers for dispersive time-varying channels: Equalization and channel acquisition," IEEE Trans. Wireless Commun., vol.52, no.4, pp.572–583, April 2004.
[6] P. Schniter, "Low-complexity equalization of OFDM in doubly selective channels," IEEE Trans. Signal Process., vol.52, no.4, pp.1002–1011, Oct. 2004.
[7] I. Barhumi, G. Leus, and M. Moonen, "Time-domain and frequency-domain per-tone equalization for OFDM over doubly selective channels," Signal Process., vol.84, no.11, pp.2055–2066, 2004.
[8] Y. Mostofi and D.C. Cox, "ICI mitigation for pilot-aided OFDM mobile systems," IEEE Trans. Wireless Commun., vol.4, no.2, pp.765–774, March 2005.
[9] L. Rugini, P. Banelli, and G. Leus, "Simple equalization of time-varying channels for OFDM," IEEE Commun. Lett., vol.9, no.7, pp.619–621, July 2005.
[10] S. Das and P. Schniter, "Max-SINR ISI/ICI-shaped multi-carrier communication over the doubly dispersive channel," IEEE Trans. Signal Process., vol.55, no.12, pp.5782–5795, Dec. 2007.
[11] D.N. Liu and M.P. Fitz, "Iterative MAP equalization and decoding in wireless mobile coded OFDM," IEEE Trans. Commun., vol.57, no.7, pp.2042–2051, July 2009.
[12] K. Fang, L. Rugini, and G. Leus, "Low-complexity block turbo equalization for OFDM systems in time-varying channels," IEEE Trans. Signal Process., vol.56, no.11, pp.5555–5566, Nov. 2008.
[13] I. Barhumi and M. Moonen, "MLSE and MAP equalization for transmission over doubly selective channels," IEEE Trans. Veh. Technol., vol.58, no.8, pp.4120–4128, Oct. 2009.
[14] T. Hrycak, S. Das, G. Matz, and H.G. Feichtinger, "Low complexity equalization for doubly selective channels modeled by a basis expansion," IEEE Trans. Signal Process., vol.58, no.11, pp.5706–5719, Nov. 2010.
[15] E. Panayirci, H. Dogan, and H.V. Poor, "Low-complexity MAP-based successive data detection for coded OFDM systems over highly mobile wireless channels," IEEE Trans. Veh. Technol., vol.60, no.6, pp.2849–2857, July 2011.
[16] Y.S. Choi, P.J. Voltz, and F.A. Cassara, "On channel estimation and detection for multicarrier signals in fast and selective Rayleigh fading channels," IEEE Trans. Commun., vol.49, no.8, pp.1375–1387, Aug. 2001.
[17] H.W. Wang, D.W. Lin, and T.H. Sang, "OFDM signal detection in doubly selective channels with blockwise whitening of residual intercarrier interference and noise," IEEE J. Sel. Areas Commun., vol.30, no.4, pp.684–694, May 2012.
[18] WiMAX Forum, "Mobile radio conformance tests amendment: Wave 2 tests," July 2007.

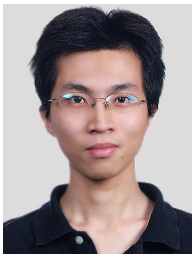

Hsin-De Lin received his B.S. degree in electronics engineering from National Chiao-Tung University, Taiwan, in 2003. He is currently working towards the Ph.D. degree in electronics engineering from National Chiao-Tung University, Taiwan. His research interests are in the area of signal processing for communications.

Tzu-Hsien Sang received the B.S.E.E. degree in 1990 from National Taiwan University and Ph.D. degree in 1999 from the University of Michigan at Ann Arbor. He is currently with the Department of Electronics Engineering, National Chiao-Tung University, Taiwan. Prior to joining NCTU in 2003, he had worked in Excess Bandwidth, a start-up company at Sunnyvale, California, working on physical layer design for broadband technologies. His research interests include signal processing for communications, time-frequency analysis for biomedical signals, and RF circuit noise modeling.

Jiunn-Tsair Chen received the Ph.D. degree in electrical engineering from Stanford University, Stanford, CA, in 1998. He was with National Tsing-Hua University, Hsinchu, Taiwan, from 1999 to 2006, during which he has published more than 100 technical papers. Since 2006, he has been with Ralink Technology Corporation, a Taiwan-based IC design house, working on wireless-MIMO-related IC products. His research interests include communication theory, antenna array signal processing, network coding, and RF/analog system calibration. He is currently with Mobile Device Corporation, Taiwan.